Topologically protected bound states in the continuum in the Su-Schrieffer-Heeger chain

Dunkan Martínez [1,*] Rodrigo P. A. Lima [2,3] Alexander López [1,4]
Francisco Domínguez-Adame [1] and Pedro A. Orellana [5]
[1]*GISC, Departamento de Física de Materiales, Universidad Complutense, E-28040 Madrid, Spain*
[2]*GISC and InterTEP, Departamento de Física, Facultad de Ciencias Ambientales y Bioquímica, Universidad de Castilla-La Mancha, E-45071 Toledo, Spain*
[3]*GFTC, Instituto de Física, Universidade Federal de Alagoas, Maceió 57072-970, AL, Brazil*
[4]*Escuela Superior Politécnica del Litoral, ESPOL, Departamento de Física, Facultad de Ciencias Naturales y Matemáticas, Campus Gustavo Galindo, Km. 30.5 Via Perimetral, P.O. Box 09-01-5863, Guayaquil, Ecuador*
[5]*Departamento de Física, Universidad Técnica Federico Santa María, Casilla 110 V, Valparaíso, Chile*

(Received 13 January 2026; accepted 23 September 2026; published 2 November 2026)

Bound states in the continuum, originally proposed within the framework of quantum mechanics, have since been observed in a variety of physical contexts, including optics, acoustics, and related fields. Of particular interest are those bound states in the continuum that are protected by continuous symmetries, as their stability makes them resistant to structural imperfections and material disorder. In this study, we demonstrate the existence of topologically protected bound states in the continuum by coupling a finite Su-Schrieffer-Heeger chain to a metallic lead. These states are characterized by distinct features in the electrical response of the system, serving as a direct indication of their topological origin. The inherent robustness of such topologically protected states highlights their potential applications in fault-tolerant quantum information processing as well as in the design of advanced electronic and photonic devices.

DOI: 10.1103/xmp6-v4zq

I. INTRODUCTION

Bound states in the continuum (BICs) are counterintuitive quantum states that, despite residing within the energy range of extended states, remain perfectly localized and decoupled from the continuum. The absence of coupling gives these states an extremely long lifetime. First introduced by von Neumann and Wigner in 1929 for quantum particles in tailored potentials [1], BICs have been identified across diverse physical platforms, including optics [2–22], acoustics [23–28], and water waves [29–31]. These states can emerge via several distinct mechanisms such as symmetry protection [4,21,22,32–36], separation of coordinate variables [14,37], parameter tuning [2,3,7–9,23–25,38], and inverse construction [5,6,29]. A key characteristic of BICs is their extremely high quality factor, which arises from their decoupling from the continuum spectrum states. Furthermore, in some cases, the quality factor can be finely tuned, making BICs attractive for use in applications such as narrow-band filters, highly sensitive sensors, and low-threshold lasers [39–45]. However, this sensitivity can also be a double-edged phenomenon: Small perturbations or imperfections can hybridize BICs with the continuum, destroying their localized nature.

On the other side, topological systems have attracted a lot of attention [46–50] due to their unique properties, such as the protection of topological states against specific classes of defects [49–52], as well as their inherent robustness for quantum computation technologies [53–60]. The recent convergence of these two concepts has given rise to a new paradigm: topological BICs (TBICs), which combine the spectral isolation of BICs with the disorder resilience of topological states [61–74].

In this work, we uncover TBICs in electron systems that arise from the coupling between a topological chain and a conventional metallic contact. Specifically, we study the effect of attaching a finite Su-Schrieffer-Heeger (SSH) chain [46] by one of its ends to a metallic lead. Despite the simplicity of the setup, we find that the SSH spectrum leaves a clear fingerprint on the lead's conductance. Most remarkably, a TBIC emerges at zero energy: a spatially confined state within the continuum, protected by the SSH chain's topology rather than by conventional parameter fine-tuning. This setup offers a minimal but robust platform for realizing TBICs in quantum systems.

II. MODEL

The system under study consists of an SSH chain of N dimer cells ($2N$ sites), which is side-coupled at one of its ends to an infinite one-dimensional lead, as shown schematically in Fig. 1. This arrangement enables the detection of SSH

*Contact author: dunmar01@ucm.es

Published by the American Physical Society under the terms of the Creative Commons Attribution 4.0 International license. Further distribution of this work must maintain attribution to the author(s) and the published article's title, journal citation, and DOI.

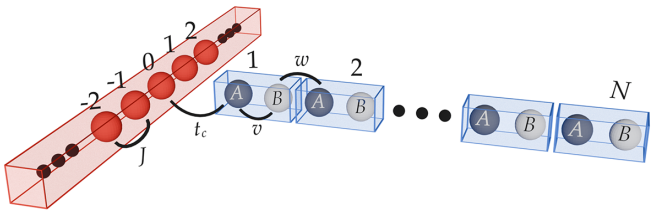


FIG. 1. Sketch of the system. The red bar represents the infinite lead, while the blue boxes show the dimer cells of the SSH chain with N cells. The spheres within the boxes represent the sites of the aforementioned elements: Red spheres correspond to the sites of the lead, while dark (light) spheres indicate sites in the sublattice A (B). Black curved lines indicate the hopping considered in our model.

chain states as antiresonances in the conductance of the lead. The system under study can be conveniently described by a tight-binding Hamiltonian given by $\mathcal{H} = \mathcal{H}_{\rm ch} + \mathcal{H}_l + \mathcal{H}_c$. Here, $\mathcal{H}_{\rm ch}$ is the Hamiltonian of the isolated SSH chain, $\mathcal{H}_l$ denotes the Hamiltonian of the isolated lead, and $\mathcal{H}_c$ stands for the coupling between the lead and the SSH chain. To be specific, these terms are defined as

$$\begin{aligned}\mathcal{H}_{ch} &= -v\sum_{\ell=1}^{N}(a_\ell^\dagger b_\ell + \text{H.c.}) - w\sum_{\ell=1}^{N-1}(b_\ell^\dagger a_{\ell+1} + \text{H.c.}),\\ \mathcal{H}_l &= -J\sum_j (c_j^\dagger c_{j+1} + \text{H.c.}),\\ \mathcal{H}_c &= -t_c c_0^\dagger a_1 + \text{H.c.}\end{aligned} \tag{1}$$

Here, c_j is the annihilation operator of an electron at site j of the lead, while a_ℓ (b_ℓ) is the annihilation operator of the SSH chain at cell ℓ and sublattice A (B). J is the hopping parameter in the lead, v is the intracell hopping in the chain while w is the intercell hopping, and t_c is the coupling parameter between the lead and the chain (see Fig. 1). We have assumed that all site energies are identical and set them to zero, without loss of generality. A more detailed description of both SSH chain and BICs along with a discussion about the chiral symmetry of the whole system after the lead is coupled is presented in Secs. S1 and S2 of the Supplemental Material [75], respectively.

Since the coupling between the lead and the chain is local, we can assume that the conductance of the system can be calculated using the Landauer-Büttiker formalism in the ballistic regime as follows:

$$G(E) = \frac{e^2}{\hbar}\left|\widehat{t}\,(E)\right|^2, \tag{2}$$

where $\widehat{t}\,(E)$ is the energy-dependent transmission amplitude at Fermi energy E and $-e$ is the electron charge. To determine the transmission amplitude, we write the wave function for each subsystem as follows:

$$\begin{aligned}\phi_j &= \begin{cases} e^{ikj} + \widehat{r}\,(E)\,e^{-ikj}, & \text{if } j<0\,,\\ \widehat{t}\,(E)\,e^{ikj}, & \text{otherwise,}\end{cases}\\ \psi_\ell &= \begin{pmatrix}\psi_\ell^A\\ \psi_\ell^B\end{pmatrix} = \widehat{\alpha}\,(E)\begin{pmatrix}1\\ e^{i\theta}\end{pmatrix}e^{iq\ell} + \widehat{\beta}\,(E)\begin{pmatrix}1\\ e^{-i\theta}\end{pmatrix}e^{-iq\ell},\end{aligned} \tag{3}$$

where ϕ_j is the wave function at the site j of the lead, while ψ_ℓ corresponds to the wave function in the cell ℓ of the chain. In addition, $\widehat{r}\,(E)$ is the energy-dependent reflection amplitude, while $\widehat{\alpha}\,(E)$ and $\widehat{\beta}\,(E)$ are the amplitude coefficients of the wave function inside the chain. Here, we have taken into account that the difference between the wave function of the two sublattices in the same cell is just a complex phase, $\exp(i\theta) = -E/[v + w\exp(-iq)]$ [76]. In addition, the wave numbers k and q can be found from the dispersion relation of the lead and chain, respectively, namely, $k = -\arccos(E/2J)$ and $q = \arccos[(E^2 - v^2 - w^2)/2vw]$. Thus, the boundary conditions for this problem can be written as

$$\begin{aligned}E\phi_{-1} &= -J(\phi_0 + \phi_{-2}),\\ E\phi_0 &= -t_c\psi_1^A - J(\phi_1 + \phi_{-1}),\\ E\psi_1^A &= -v\psi_1^B - t_c\phi_0,\\ E\psi_N^B &= -v\psi_N^A.\end{aligned} \tag{4}$$

After some lengthy but straightforward calculations (see Sec. S3 of the Supplemental Material [75]), the transmission amplitude is found to be given by

$$\widehat{t}(E) = \frac{1}{1 - i\Gamma\dfrac{\sin[q(E)N]}{\sin k(E)\sin[q(E)(N+1) - \theta(E)]}}, \tag{5}$$

where $\Gamma = t_c^2/2Jw$ is an energy-independent parameter in the wide-band limit describing the effective hopping between the SSH chain and the lead. Once we know the expression for the transmission coefficient, we can find the values of the parameters α and β to obtain the electron wave function in the chain ψ_ℓ. This can be used to find the density of the states (DOS) in the chain as $\rho^{\rm ch}(E) \sim \sum_{\ell\in{\rm chain}}\{|\psi_\ell^A(E)|^2 + |\psi_\ell^B(E)|^2\}$.

III. TOPOLOGICAL BIC

From Eq. (5), we can see that the transmission at the Fermi energy can be tuned by the parameters v, which effectively controls the occurrence of the topological state of the chain, and Γ. For the present study, we consider w as a unit of energy. Therefore, the topological state arises if $v < w$. As we are dealing with a perfect lead with an SSH chain attached to it, we expect the transmission to be unity for all energies except the ones that match the energy spectra of the latter [see Fig. 2(a)].

We see from the results shown in Fig. 2(b) that the DOS remains almost independent of energy except near $E = 0$, where a resonance appears, exhibiting the expected behavior of a TBIC. This TBIC comes from the exponential decay that characterizes the topological state in the SSH chain. When v is close to zero, the exponential decay is very abrupt, causing the wave functions at either end to barely overlap. This fact allows us to combine both topological states in a symmetric and an antisymmetric way, resulting in a state that is effectively disconnected from the lead.

Since the TBIC originates from the proximity of the lead to one of the ends of the chain, it will be protected as long as the topology of the SSH chain remains; i.e., perturbations such as disorder in the chain hoppings or an increased coupling strength between the chain and the lead do not cause the TBIC to leak. To demonstrate this robustness, disorder

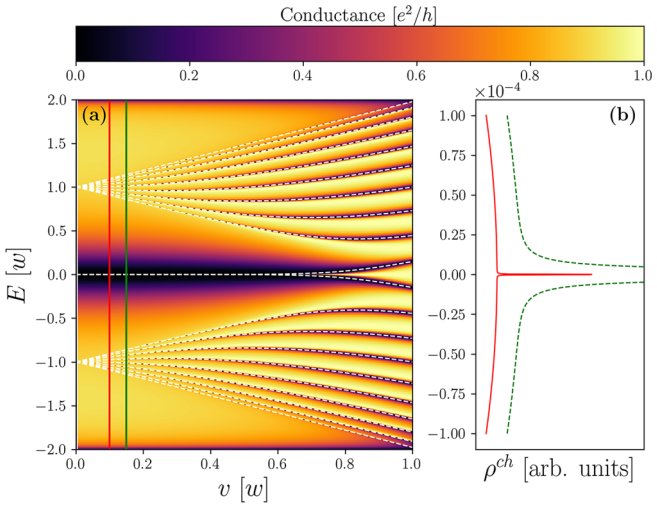


FIG. 2. Conductance and DOS of an SSH chain of $N = 10$ cells hanged to the lead; Γ has been set to 0.3 and $J = w$. (a) Conductance in units of e^2/h; in white dashed lines, the spectra of the SSH has been plotted. Vertical lines represent the value of v, where the DOS has been calculated. (b) DOS in arbitrary units for $v = 0.1w$ (red solid line) and $v = 0.15w$ (green dashed line) near $E = 0$ (notice the energy scale factor).

is introduced by adding to each hopping a random value drawn from a uniform probability distribution over the interval $[-W/2, W/2]$. As shown in Fig. 3, the zero-conductance regions are progressively smeared out as the disorder strength W increases. Nevertheless, the one centered at zero energy remains unaffected for large magnitudes of disorder, which proves the topological protection of this state.

To explain the emergence of TBICs, we consider an effective model, similar to that presented in Refs. [77,78], in which the influence of the infinite lead is embodied through a renormalized site with complex self-energy ε_L, coupled via an effective coupling constant ξ to the two topological states of the SSH chain with energies $\mu \pm \delta$ (see Fig. 4). The effective

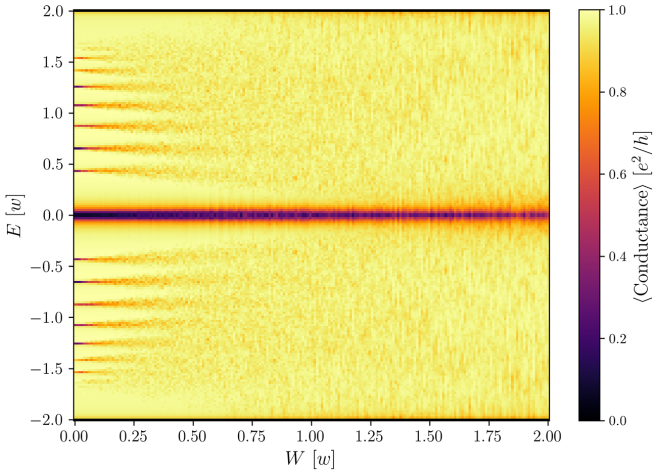


FIG. 3. Average conductance in units of e^2/h of an SSH chain of $N = 10$ cells averaged over $M = 50$ disorder realizations, as a function of the Fermi energy and the magnitude of disorder W. The pristine value of v has been set to $0.7w$ and $J = w$.

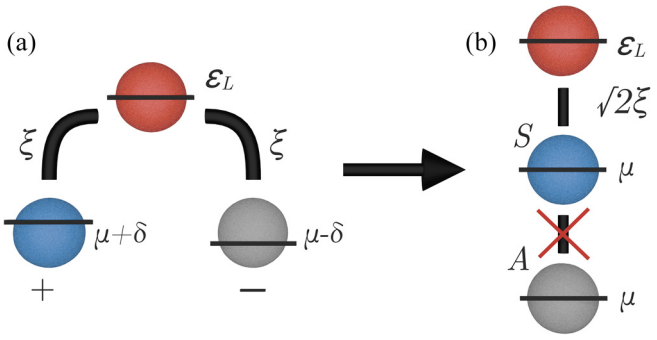


FIG. 4. Sketch of the effective model that illustrates the formation of the TBIC. (a) The entire lead is effectively replaced by a single site with complex energy ε_L that is coupled with coupling constant ξ to two topological states with energies $\mu \pm \delta$ (see main text for an explanation). (b) After performing a unitary transformation, the antisymmetric state A is decoupled from the rest of the states, and it can be regarded as a TBIC.

Hamiltonian reads

$$H_{\text{eff}} = \varepsilon_L|L\rangle\langle L| + (\mu+\delta)|\psi_+\rangle\langle\psi_+| + (\mu-\delta)|\psi_-\rangle\langle\psi_-| - \xi|L\rangle\Big(\langle\psi_+| + \langle\psi_-|\Big) - \xi^*\Big(|\psi_+\rangle + |\psi_-\rangle\Big)\langle L| \,. \quad (6)$$

By performing a linear transformation to the symmetric and antisymmetric states $|\psi_S\rangle = (1/\sqrt{2})(|\psi_+\rangle + |\psi_-\rangle)$ and $|\psi_A\rangle = (1/\sqrt{2})(|\psi_+\rangle - |\psi_-\rangle)$, and taking the limit $\delta \to 0$, i.e., the topological regime, the Hamiltonian takes the form

$$H_{\text{eff}} = \varepsilon_L|L\rangle\langle L| + \mu|\psi_S\rangle\langle\psi_S| + \mu|\psi_A\rangle\langle\psi_A| - \sqrt{2}\xi|L\rangle\langle\psi_S| - \sqrt{2}\xi^*|\psi_S\rangle\langle L| \,. \quad (7)$$

Therefore, the antisymmetric state is an eigenstate of the entire system and thus a TBIC, a bound state in the continuum protected by the system's topology. Figure 4 shows a sketch of the effective model that illustrates the formation of TBICs through the linear transformation described above. In Sec. S4 of the Supplemental Material [75], the DOS of the effective model has been calculated to show that it holds TBICs.

IV. DYNAMICS OF THE TBICs

The localized nature of the state can be assessed by the time evolution (we take $\hbar = 1$ hereafter) of a wave packet initially localized at one of three representative sites within the SSH chain: the nearest site to the lead; where the wave function amplitude decays exponentially as it leaks into the lead, a second site within the bulk of the chain, where the dynamics consists of multiple reflections between the inner boundaries of the chain, producing Fabry-Perot-like interference; and finally, at the farthest site where the TBIC is located, the wave function should remain localized and time invariant.

Figure 5 displays the time evolution for the three initial conditions described above. The red line corresponds to the site nearest to the lead, where the probability amplitude decays approximately exponentially as it couples to the continuum. The blue line represents a state initialized at the farthest boundary of the SSH bulk, which propagates along the chain and undergoes Fabry-Perot-like reflections, leading to

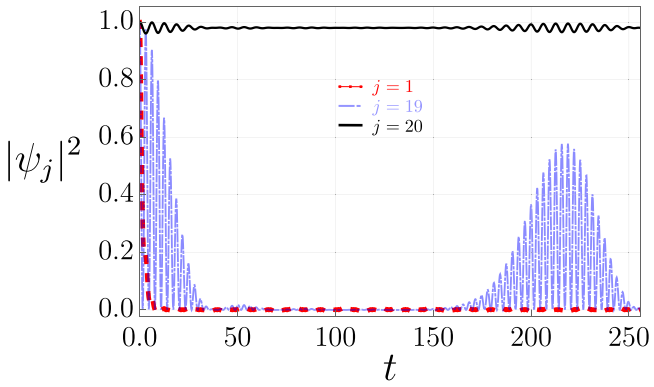


FIG. 5. Return probability as a function of time of two topological states (dotted red and solid black curves) and one trivial state (dashed blue curve) in an SSH chain of $N = 10$ dimer cells attached to a lead consisting of 601 sites, with $\Gamma = 0.3$, $J = w$, and $v = 0.1w$, for three specific sites: $j = 1$ (dotted red line), $j = 19$ (dashed blue line), and $j = 20$ (solid black line). Time is expressed in units of w^{-1}.

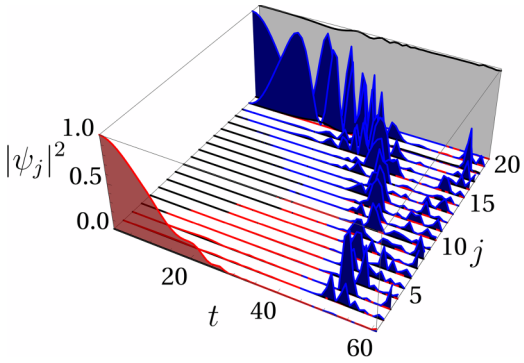


FIG. 6. Probability density of two topological states (red and black curves) and one trivial state (blue curve) on an SSH chain of $N = 10$ dimer cells attached to a lead consisting of 601 sites, with $\Gamma = 0.3$, $J = w$, and $v = 0.1w$, for three specific sites: $j = 1$ (red line), $j = 19$ (blue line), and $j = 20$ (black line). Time is expressed in units of w^{-1}.

maxima in the probability of site occupation, with a periodicity of approximately $220w^{-1}$ (in Fig. S7 of the Supplemental Material [75], we show that the dynamical evolution of any other bulk state is qualitatively similar to that of the $j = 19$ state). Finally, the black curve corresponds to the BIC located at the farthest end, slight initial decay is observed due to leakage in the bulk, consistent with the finite value of the coupling parameter v, and subsequent scattering with the bulk states occurs when their Fabry-Perot maxima coincide, giving rise to a small-amplitude beating.The behavior of the probability as a function of time, depending on the initial condition, can be explained as follows. If the initial condition is that the particle is in the site $j = 1$ (red line in Fig. 5), the closest site to the infinite lead, the state of the system corresponds closely to the symmetrical state; this state is strongly coupled to the continuum. It decays exponentially with a rate γ, with a beating that takes into account the coupling with the rest of the sites of the SSH chain. As a consequence, the probability of this site, $P_{\text{trivial}}(t)$, is proposed as a phenomenological ansatz:

$$P_{\text{trivial}}(t) = \Big(a\cos^2(wt) + b\Big)e^{-\gamma t}, \tag{8}$$

where a, b, and γ are parameters such that $a + b = 1$.

On the other hand, the initial condition corresponding to the particle localized in $j = 19$ (blue line) shows that the particle feels a trivial chain with loss, coupled to a localized state. The behavior of the return probability can be explained by a phenomenological model in which we consider a uniform chain with diagonal losses. By directly using the well-known analytical solution for the eigenstates and eigenvalues of such a uniform tight-binding chain of length N, the probability of finding a particle at the site $j = 19$ at $t > 0$ ($P_{\text{bulk}}(t)$) is given by the following equation:

$$P_{\text{bulk}}(t) = \cos^2(wt)\left|\sum_{n=1}^{N} c_n e^{-i\varepsilon_n t} e^{-\Gamma_n t}\right|^2, \tag{9}$$

where $c_n = 2/(N+1)\sin[n\pi/(N+1)]$, $\varepsilon_n = -2v\cos[n\pi/(N+1)]$, and $\Gamma_n = [V_0^2/v_c(N+1)]\sin[n\pi(N+1)]$. In this case, the particle is scattered and partially reflected at the SSH-lead junction. This backscattering effect accounts for the second peak in the probability distribution around $t = 220w^{-1}$.

Finally, if the particle is initially located at the end of the chain, it is almost in an antisymmetric state, indicating that it occupies a BIC. By employing a minimal model with two dimers as a closed system and expanding the states of the system in terms of its eigenstates, we can determine the probability of finding the particle at the end site of the chain ($P_{\text{TBIC}}(t)$) as

$$P_{\text{TBIC}}(t) = \frac{1 + 2\lambda^2\cos(wt)\cos(v\lambda t) + \lambda^4\cos(wt)}{(1+\lambda^2)^2}, \tag{10}$$

where λ is the ratio v/w. The numerical evaluation of the above equations and the comparison with the results shown in Fig. 5 can be found in Sec. S5 of the Supplemental Material [75].

Figure 6 shows the probability density as a function of time and space for the same three initial conditions in Fig. 5. For $j = 1$ (red line), the probability decays exponentially in the continuum without coupling with the rest of the chain. In contrast, when the wave packet is initially located in the bulk (at $j = 19$, represented by the blue lines), it oscillates back and forth due to the system's finite size. This bouncing behavior explains the non-Markovian nature of the probability. For $j = 20$, the particle remains primarily localized at the end of the chain, exhibiting weak oscillations due to its coupling with the nearest neighbors. As a result, the particle is found in a TBIC and does not decay into the continuum.

V. CONCLUSIONS

In summary, we demonstrate the existence of topologically protected BICs in an SSH chain. Their robustness originates from a topological obstruction that forbids hybridization with extended states, ensuring their persistence without parameter fine-tuning. We further show that these states can be unambiguously identified via electrical transport measurements, whose dynamical response provides direct signatures of their

properties. Photonic and acoustic platforms offer promising routes for realizing TBICs. Based on the analogy of topological photonics and condensed matter systems [79], Real *et al.* have experimentally demonstrated the excitation of edge modes in an SSH photonic lattice [80]. Conventional BICs are widely employed in applications involving trapped light and sound due to their high quality factor. However, they are notably sensitive to external perturbations. In contrast, TBICs exhibit greater robustness against weak perturbations, leading to more stable and efficient particle confinement and highlighting their significance as resilient excitations embedded in the continuum, with important implications for electron transport and wave-control phenomena, such as high-fidelity qubit readout or applications involving trapped light.

ACKNOWLEDGMENTS

Work at Madrid has been supported by Comunidad de Madrid (Recovery, Transformation and Resilience Plan) and NextGenerationEU from the European Union (Grant No. MAD2D-CM-UCM5) and Agencia Estatal de Investigación (Grant No. PID2022-136285NB-C31/3). D.M. acknowledges financial support from the Comunidad de Madrid (Consejería de Educación, Ciencia y Universidades) under the Predoctoral Research Training Program (Grant No. PIPF-2023/TEC-30208). P.A.O. acknowledges support from DGIIE USM PI-LIR-26-10, FONDECYT Grants No. 122070 and No. 1230933. R.P.A.L. acknowledges financial support from BG23/00151 action (MCINU and UCLM, Spain). We acknowledge helpful discussions with R. A. Molina and S. Bravo.

DATA AVAILABILITY

The data that support the findings of this article are not publicly available. The data are available from the authors upon reasonable request.

[1] J. von Neumann and E. P. Wigner, Über merkwürdige diskrete Eigenwerte, in *The Collected Works of Eugene Paul Wigner*, edited by A. S. Wightman (Springer, Berlin, Heidelberg, 1993), pp. 291–293.

[2] E. N. Bulgakov and A. F. Sadreev, Bound states in the continuum in photonic waveguides inspired by defects, Phys. Rev. B **78**, 075105 (2008).

[3] D. C. Marinica, A. G. Borisov, and S. V. Shabanov, Bound states in the continuum in photonics, Phys. Rev. Lett. **100**, 183902 (2008).

[4] Y. Plotnik, O. Peleg, F. Dreisow, M. Heinrich, S. Nolte, A. Szameit, and M. Segev, Experimental observation of optical bound states in the continuum, Phys. Rev. Lett. **107**, 183901 (2011).

[5] M. I. Molina, A. E. Miroshnichenko, and Y. S. Kivshar, Surface bound states in the continuum, Phys. Rev. Lett. **108**, 070401 (2012).

[6] G. Corrielli, G. Della Valle, A. Crespi, R. Osellame, and S. Longhi, Observation of surface states with algebraic localization, Phys. Rev. Lett. **111**, 220403 (2013).

[7] C. W. Hsu, B. Zhen, J. Lee, S.-L. Chua, S. G. Johnson, J. D. Joannopoulos, and M. Soljačić, Observation of trapped light within the radiation continuum, Nature (London) **499**, 188 (2013).

[8] S. Weimann, Y. Xu, R. Keil, A. E. Miroshnichenko, A. Tünnermann, S. Nolte, A. A. Sukhorukov, A. Szameit, and Y. S. Kivshar, Compact surface Fano states embedded in the continuum of waveguide arrays, Phys. Rev. Lett. **111**, 240403 (2013).

[9] F. Monticone and A. Alù, Embedded photonic eigenvalues in 3D nanostructures, Phys. Rev. Lett. **112**, 213903 (2014).

[10] Y. Yang, C. Peng, Y. Liang, Z. Li, and S. Noda, Analytical perspective for bound states in the continuum in photonic crystal slabs, Phys. Rev. Lett. **113**, 037401 (2014).

[11] B. Zhen, C. W. Hsu, L. Lu, A. Douglas Stone, and M. Soljačić, Topological nature of optical bound states in the continuum, Phys. Rev. Lett. **113**, 257401 (2014).

[12] R. A. Vicencio, C. Cantillano, L. Morales-Inostroza, B. Real, C. Mejía-Cortés, S. Weimann, A. Szameit, and M. I. Molina, Observation of localized states in Lieb photonic lattices, Phys. Rev. Lett. **114**, 245503 (2015).

[13] S. Mukherjee, A. Spracklen, D. Choudhury, N. Goldman, P. Öhberg, E. Andersson, and R. R. Thomson, Observation of a localized flat-band state in a photonic Lieb lattice, Phys. Rev. Lett. **114**, 245504 (2015).

[14] N. Rivera, C. W. Hsu, B. Zhen, H. Buljan, J. D. Joannopoulos, and M. Soljačić, Controlling directionality and dimensionality of radiation by perturbing separable bound states in the continuum, Sci. Rep. **6**, 33394 (2016).

[15] J. Gomis-Bresco, D. Artigas, and L. Torner, Anisotropy-induced photonic bound states in the continuum, Nat. Photon. **11**, 232 (2017).

[16] S. I. Azzam, V. M. Shalaev, A. Boltasseva, and A. V. Kildishev, Formation of bound states in the continuum in hybrid plasmonic-photonic systems, Phys. Rev. Lett. **121**, 253901 (2018).

[17] A. Cerjan, C. W. Hsu, and M. C. Rechtsman, Bound states in the continuum through environmental design, Phys. Rev. Lett. **123**, 023902 (2019).

[18] S. I. Azzam and A. V. Kildishev, Photonic bound states in the continuum: From basics to applications, Adv. Opt. Mater. **9**, 2001469 (2021).

[19] Q. Song, Z. Yi, H. Xiang, and D. Han, Dynamics and asymmetric behavior of loss-induced bound states in the continuum in momentum space, Phys. Rev. B **107**, 165142 (2023).

[20] S. Pinto, R. A. Molina, and P. A. Orellana, Bound states in the continuum in asymmetric crossbar junctions in one-dimensional waveguides, Phys. Rev. A **110**, 013501 (2024).

[21] A. R. Legón, M. Ahumada, J. P. Ramos-Andrade, R. A. Molina, and P. A. Orellana, Bound states in the continuum in a double whispering-gallery resonator, Phys. Rev. A **111**, 013529 (2025).

[22] D. Martínez, P. A. Orellana, L. Rosales, J. Dolado, M. Amado, E. Diez, F. Domínguez-Adame, and R. P. A. Lima, Uncover-

ing bound states in the continuum in InSb nanowire networks, Physica E **166**, 116145 (2025).
[23] A. Lyapina, D. Maksimov, A. Pilipchuk, and A. Sadreev, Bound states in the continuum in open acoustic resonators, J. Fluid Mech. **780**, 370 (2015).
[24] S. Huang, T. Liu, Z. Zhou, X. Wang, J. Zhu, and Y. Li, Extreme sound confinement from quasibound states in the continuum, Phys. Rev. Appl. **14**, 021001 (2020).
[25] L. Huang, Y. K. Chiang, S. Huang, C. Shen, F. Deng, Y. Cheng, B. Jia, Y. Li, D. A. Powell, and A. E. Miroshnichenko, Sound trapping in an open resonator, Nat. Commun. **12**, 4819 (2021).
[26] I. Deriy, I. Toftul, M. Petrov, and A. Bogdanov, Bound states in the continuum in compact acoustic resonators, Phys. Rev. Lett. **128**, 084301 (2022).
[27] S. Yin, L. Ye, H. He, X. Huang, M. Ke, W. Deng, J. Lu, and Z. Liu, Valley edge states as bound states in the continuum, Sci. Bull. **69**, 1660 (2024).
[28] L. Huang, S. Huang, C. Shen, S. Yves, A. S. Pilipchuk, X. Ni, S. Kim, Y. K. Chiang, D. A. Powell, J. Zhu, Y. Cheng, Y. Li, A. F. Sadreev, A. Alù, and A. E. Miroshnichenko, Acoustic resonances in non-Hermitian open systems, Nat. Rev. Phys. **6**, 11 (2024).
[29] M. McIver, An example of non-uniqueness in the two-dimensional linear water wave problem, J. Fluid Mech. **315**, 257 (1996).
[30] C. Linton and P. McIver, Embedded trapped modes in water waves and acoustics, Wave Motion **45**, 16 (2007).
[31] L.-P. Euvé, K. Pham, R. Porter, P. Petitjeans, V. Pagneux, and A. Maurel, Perfect resonant absorption of guided water waves by Autler-Townes splitting, Phys. Rev. Lett. **131**, 204002 (2023).
[32] M. L. L. de Guevara and P. A. Orellana, Electronic transport through a parallel-coupled triple quantum dot molecule: Fano resonances and bound states in the continuum, Phys. Rev. B **73**, 205303 (2006).
[33] R. Parker, Resonance effects in wake shedding from parallel plates: Some experimental observations, J. Sound Vib. **4**, 62 (1966).
[34] N. Cumpsty and D. Whitehead, The excitation of acoustic resonances by vortex shedding, J. Sound Vib. **18**, 353 (1971).
[35] D. V. Evans, M. Levitin, and D. Vassiliev, Existence theorems for trapped modes, J. Fluid Mech. **261**, 21 (1994).
[36] J. Mur-Petit and R. A. Molina, Chiral bound states in the continuum, Phys. Rev. B **90**, 035434 (2014).
[37] J. U. Nöckel, Resonances in quantum-dot transport, Phys. Rev. B **46**, 15348 (1992).
[38] D. Braak, L. Cong, H.-P. Eckle, H. Johannesson, and E. K. Twyeffort, Spectral continuum in the Rabi–Stark model [Invited], J. Opt. Soc. Am. B **41**, C97 (2024).
[39] C. W. Hsu, B. Zhen, A. D. Stone, J. D. Joannopoulos, and M. Soljačić, Bound states in the continuum, Nat. Rev. Mater. **1**, 16048 (2016).
[40] A. Kodigala, T. Lepetit, Q. Gu, B. Bahari, Y. Fainman, and B. Kanté, Lasing action from photonic bound states in continuum, Nature (London) **541**, 196 (2017).
[41] M.-S. Hwang, H.-C. Lee, K.-H. Kim, K.-Y. Jeong, S.-H. Kwon, K. Koshelev, Y. Kivshar, and H.-G. Park, Ultralow-threshold laser using super-bound states in the continuum, Nat. Commun. **12**, 4135 (2021).
[42] J.-H. Yang, Z.-T. Huang, D. N. Maksimov, P. S. Pankin, I. V. Timofeev, K.-B. Hong, H. Li, J.-W. Chen, C.-Y. Hsu, Y.-Y. Liu, T.-C. Lu, T.-R. Lin, C.-S. Yang, and K.-P. Chen, Low-threshold bound state in the continuum lasers in hybrid lattice resonance metasurfaces, Laser Photonics Rev. **15**, 2100118 (2021).
[43] S. Mohamed, J. Wang, H. Rekola, J. Heikkinen, B. Asamoah, L. Shi, and T. K. Hakala, Controlling topology and polarization state of lasing photonic bound states in continuum, Laser Photonics Rev. **16**, 2100574 (2022).
[44] M.-S. Hwang, K.-Y. Jeong, J.-P. So, K.-H. Kim, and H.-G. Park, Nanophotonic nonlinear and laser devices exploiting bound states in the continuum, Commun. Phys. **5**, 106 (2022).
[45] B. Liu, Y. Peng, Z. Jin, X. Wu, H. Gu, D. Wei, Y. Zhu, and S. Zhuang, Terahertz ultrasensitive biosensor based on wide-area and intense light-matter interaction supported by QBIC, Chem. Eng. J. **462**, 142347 (2023).
[46] W. P. Su, J. R. Schrieffer, and A. J. Heeger, Solitons in polyacetylene, Phys. Rev. Lett. **42**, 1698 (1979).
[47] M. Z. Hasan and C. L. Kane, *Colloquium*: Topological insulators, Rev. Mod. Phys. **82**, 3045 (2010).
[48] X.-L. Qi and S.-C. Zhang, Topological insulators and superconductors, Rev. Mod. Phys. **83**, 1057 (2011).
[49] L. Lu, J. D. Joannopoulos, and M. Soljačić, Topological photonics, Nat. Photon. **8**, 821 (2014).
[50] H. Xue, Y. Yang, and B. Zhang, Topological acoustics, Nat. Rev. Mater. **7**, 974 (2022).
[51] G. Ma, M. Xiao, and C. T. Chan, Topological phases in acoustic and mechanical systems, Nat. Rev. Phys. **1**, 281 (2019).
[52] D. Martínez, Álvaro Díaz-Fernández, P. A. Orellana, and F. Domínguez-Adame, Anomalous spin textures in a 2D topological superconductor induced by point impurities, Ann. Phys. **535**, 2300072 (2023).
[53] A. Kitaev, Fault-tolerant quantum computation by anyons, Ann. Phys. **303**, 2 (2003).
[54] P. Milman and R. Mosseri, Topological phase for entangled two-qubit states, Phys. Rev. Lett. **90**, 230403 (2003).
[55] C. E. R. Souza, J. A. O. Huguenin, P. Milman, and A. Z. Khoury, Topological phase for spin-orbit transformations on a laser beam, Phys. Rev. Lett. **99**, 160401 (2007).
[56] L. E. Oxman and A. Z. Khoury, Fractional topological phase for entangled qudits, Phys. Rev. Lett. **106**, 240503 (2011).
[57] M. Johansson, M. Ericsson, K. Singh, E. Sjöqvist, and M. S. Williamson, Topological phases and multiqubit entanglement, Phys. Rev. A **85**, 032112 (2012).
[58] A. A. Matoso, X. Sánchez-Lozano, W. M. Pimenta, P. Machado, B. Marques, F. Sciarrino, L. E. Oxman, A. Z. Khoury, and S. Pádua, Experimental observation of fractional topological phases with photonic qudits, Phys. Rev. A **94**, 052305 (2016).
[59] S. A. Hassani Gangaraj, C. Valagiannopoulos, and F. Monticone, Topological scattering resonances at ultralow frequencies, Phys. Rev. Res. **2**, 023180 (2020).
[60] I. Katsantonis, A. C. Tasolamprou, T. Koschny, E. N. Economou, M. Kafesaki, and C. Valagiannopoulos, Giant enhancement of nonreciprocity in gyrotropic heterostructures, Sci. Rep. **13**, 21986 (2023).
[61] B.-J. Yang, M. Saeed Bahramy, and N. Nagaosa, Topological protection of bound states against the hybridization, Nat. Commun. **4**, 1524 (2013).
[62] Y.-X. Xiao, G. Ma, Z.-Q. Zhang, and C. T. Chan, Topological subspace-induced bound state in the continuum, Phys. Rev. Lett. **118**, 166803 (2017).

[63] M. Takeichi and S. Murakami, Topological linelike bound states in the continuum, Phys. Rev. B **99**, 035128 (2019).

[64] A. Cerjan, M. Jürgensen, W. A. Benalcazar, S. Mukherjee, and M. C. Rechtsman, Observation of a higher-order topological bound state in the continuum, Phys. Rev. Lett. **125**, 213901 (2020).

[65] W. A. Benalcazar and A. Cerjan, Bound states in the continuum of higher-order topological insulators, Phys. Rev. B **101**, 161116 (2020).

[66] Z. Li, J. Wu, X. Huang, J. Lu, F. Li, W. Deng, and Z. Liu, Bound state in the continuum in topological inductor–capacitor circuit, Appl. Phys. Lett. **116**, 263501 (2020).

[67] J. D. H. Rivero, C. Fleming, B. Qi, L. Feng, and L. Ge, Robust zero modes in non-Hermitian systems without global symmetries, Phys. Rev. Lett. **131**, 223801 (2023).

[68] L. Liu, T. Li, Q. Zhang, M. Xiao, and C. Qiu, Universal mirror-stacking approach for constructing topological bound states in the continuum, Phys. Rev. Lett. **130**, 106301 (2023).

[69] Z. Wang, X. Wang, Z. Hu, D. Bongiovanni, D. Jukić, L. Tang, D. Song, R. Morandotti, Z. Chen, and H. Buljan, Subsymmetry-protected topological states, Nat. Phys. **19**, 992 (2023).

[70] X. Wang, D. Bongiovanni, Z. Wang, A. Abdrabou, Z. Hu, D. Jukić, D. Song, R. Morandotti, R. El-Ganainy, Z. Chen, and H. Buljan, Construction of topological bound states in the continuum via subsymmetry, ACS Photonics **11**, 3213 (2024).

[71] R. Dong, Y. Zhu, D. Mao, X. Wang, and Y. Li, Observation of extreme anisotropic sensitivity at topological bound states in the continuum, Phys. Rev. Lett. **134**, 206601 (2025).

[72] S. Yin, Z. Wang, L. Ye, H. He, M. Ke, W. Deng, J. Lu, and Z. Liu, Dimensional hierarchy of topological bound states in the continuum, Phys. Rev. Lett. **135**, 126602 (2025).

[73] E. N. Bulgakov and D. N. Maksimov, Topological bound states in the continuum in arrays of dielectric spheres, Phys. Rev. Lett. **118**, 267401 (2017).

[74] L. Huang, B. Jia, Y. K. Chiang, S. Huang, C. Shen, F. Deng, T. Yang, D. A. Powell, Y. Li, and A. E. Miroshnichenko, Topological supercavity resonances in the finite system, Adv. Sci. **9**, 2200257 (2022).

[75] See Supplemental Material at http://link.aps.org/supplemental/10.1103/xmp6-v4zq for full details of the calculations for the relevant quantities.

[76] A. Bissonnette, N. Delnour, A. Mckenna, H. Eleuch, M. Hilke, and R. MacKenzie, Boundary-induced topological transition in an open Su-Schrieffer-Heeger model, Phys. Rev. B **109**, 075106 (2024).

[77] D. Zhang, S. Xia, W. Xu, X. Zhai, and L. Wang, Topological plasmonically induced transparency in a graphene waveguide system, Phys. Rev. B **109**, 245420 (2024).

[78] D. Zhang, X. Zhai, and S. Xia, Topological edge modes enable plasmon-induced transparency in isotropic and anisotropic 2D materials, Opt. Express **33**, 26974 (2025).

[79] Á. Buendía, J. A. Sánchez-Gil, and V. Giannini, Exploiting oriented field projectors to open topological gaps in plasmonic nanoparticle arrays, ACS Photonics **10**, 464 (2023).

[80] B. Real, D. Guzmán-Silva, and R. A. Vicencio, Radiation-based wave-packet generator in one-dimensional lattices, Phys. Rev. B **109**, 064308 (2024).